Open access • Posted Content • DOI:10.1007/S00339-021-05026-2

Influence of B-site Gd+3 substitution on various properties of Co-ferrite nanoparticles

Manoj Salgaonkar, Rajendra S. Gad

Institutions: St. Xavier's College-Autonomous, Mumbai, Goa University

Published on: 24 Jun 2021 - Applied Physics A (Springer Science and Business Media LLC)

Topics: Ferrite (magnet), Lattice constant, Nanocrystalline material, Crystallite and Dielectric

Influence of B-Site Gd^{+3} Substitution on Various Properties of Co-Ferrite Nanoparticles

Manoj Salgaonkar (mantejsal.unigoa@gmail.com)
St. Xavier's College, Mapusa
R. S. Gad
Goa University

Research Article

Keywords: Ferrite nanoparticles, lattice constant, saturation magnetization, DC resistivity, dielectric constant

Posted Date: June 24th, 2021

DOI: https://doi.org/10.21203/rs.3.rs-640949/v1

Version of Record: A version of this preprint was published at Applied Physics A on October 24th, 2021. See the published version at https://doi.org/10.1007/s00339-021-05026-2.

Abstract

The effect of rare earth (Gd^{+3}) substitution on various properties of nanocrystalline cobalt ferrite material with composition $CoFe_{2-x}Gd_xO$ (x = 0, 0.02, 0.04, 0.06, 0,08, 0.1) prepared using combustion method was investigated. The alterations produced in the structural parameters of the spinel lattice of cobalt ferrite were investigated using X-ray diffraction (XRD). The structural parameter such as Lattice constant, mass density, strain, and crystallite size showed irregular variation triggered due to Rare earth inclusion. The chemical composition analysis was done using energy-dispersive X-ray spectroscopy (EDS). Morphological investigations were done using a scanning electron microscope (SEM). The dependence of A.C. susceptibility and other crucial magnetic properties on rare earth content in the ferrite matrix was also investigated. The temperature dependence of electrical properties such as DC resistivity, dielectric constant, and dielectric loss was also investigated to study the alterations caused due to incorporation of rare earth ions.

Introduction

The remarkable advancement in the research based on magnetic nanoparticles such as Co ferrite, Ni ferrite, Mn Zn ferrite, and numerous combinations of transition and inner transition metal oxides in the last two decades is mainly due to their promising application in ferrofluid technology, biomedical sensors, advanced magnetic storage technology, electromagnetic interference suppression technology, targeted drug delivery systems and hyperthermia [1–3]. In recent times cobalt ferrite in its nano dimensional form has been subjected to extensive investigations mainly because of properties structural, electrical, and magnetic properties that are highly tuneable and has been done using various factors such as different dopant ions, radiation exposure, pressure, and heat treatment, etc. It belongs to the cubic spinel (AB_2O_4) family with Fe^{+3} ions occupying the octahedral site (B site) and Co^{+2} occupying the tetrahedral site [5–10].

The effects of substitution of rare earth elements such as La^{+3}, Ce^{+3}, Nd^{+3}, Gd^{+3}, Sm^{+3}, Er^{+3}, Ho^{+3}, $Dy^{+3,}$ etc. on various combinations of ferrites have been extensively studied. According to the reports, even a minute substitution affects structural, electrical, and magnetic properties significantly. These property alterations have been attributed to larger ionic radii, magnetic ordering in rare earth metal ions [10–19].

However, it is difficult to substitute a larger quantity of rare earth dopant ions due to the large size and tendency to occupy the octahedral site replacing the smaller Fe^{+3} ions which may lead to the formation of a secondary phase [20–27]. Numerous methods are being employed by researchers all over the globe to synthesize ferrite nanoparticles. Methods such as the co-precipitation method, Hydrothermal synthesis, Sol-gel method are very frequently used methods. The selection of a suitable method for material synthesis is done based upon various parameters such as yield percentage, purity of phase, energy consumption, the time required for the synthesis, and repeatability [25–31]. Compared to these material preparation methods, the combustion method appears to be the most ensuring method because of its utmost simplicity, high productivity, cost-effectiveness, and approximate control over the factors such as

size, morphology, composition, and agglomeration degree by varying the experimental conditions such as temperature, time, reactants, and stirring rate [28–32].

In this study, we intend to report the effect of increasing rare earth (Gd^{+3}) substitution on structural, morphological, elemental, and electrical properties of cobalt ferrites with composition $CoFe_{2-x}Gd_xO_4$ (x restricted to 5% to reduce the chances of secondary phase formation) nanoparticles prepared using combustion method.

1.2 Material Preparation

The nanoparticles of Gd^{+3} doped cobalt ferrite powders with chemical formula $CoFe_{2-x}Gd_xO_4$ (x = 0.0, 0.02, 0.04, 0.05, 0.06, 0.08 and, 0.1) were prepared using combustion method [30]. The metal salts such as Cobaltous (II) nitrates ($Co(NO_3)_26H_2O$), Ferric (III) nitrate nonahydrate ($Fe(NO_3)_39H_2O$), and Gadolinium acetate were dissolved in double distilled water along with nitrilotriacetic acid ($N(CH_2CO_2H)_3$) as complexing agents and urea ($CO(NH_2)_2$) as fuel. The clear solution obtained from the mixture of the above reagents heated at an elevated temperature of 90^oC was heated further till the ignition temperature is reached. The dry residue obtained as a result of the combustion process was finely crushed and ground for two hours to obtained ferrite nano-powders [21, 25, 27–28].

1.3 Material characterization

The nanocrystalline samples with composition $CoFe_{2-x}Gd_xO_4$ (x = 0.0, 0.02, 0.04, 0.06, 0.08, 0.1) prepared using combustion synthesis were analyzed using several experimental investigations. The X-ray diffraction (XRD) patterns were obtained on the Rigaku X-Ray diffractometer (Cu Kα, λ = 1.5418 Å) in 2θ scanning range of 20^o to 80^o with a step size of 0.02^o. Rietveld refinement on the XRD patterns was carried out using Full Prof software. The Fourier transforms infrared spectra of Gd^{+3} doped cobalt ferrite nanoparticles were recorded on Shimadzu FTIR 8900 setup using KBr pellets (diameter 1.5mm, radius 5mm) containing 2mg of the sample. The Scanning electron microscope (SEM) Carl Zeiss EVO18 was used to obtain surface images of ferrite nanoparticles. The Hitachi transmission electron microscope was employed to obtain images of ferrite material. The variation of normalized AC susceptibility with the temperature of rare earth doped cobalt ferrite samples was studied using the high temperature AC susceptibility set up supplied by ADEC Embedded Technology & Solutions Pvt Ltd. Magnetic hysteresis data was recorded on Quantum Design Versa Lab's 3T vibrating sample magnetometer (VSM)The samples were pressed into pellets of diameter 5 mm and thickness 2.5 mm with an approximate weight of 0.75g and were used to investigate electrical properties. The dielectric constant 'ε' variation with frequency of applied field (10Hz to 3MHz) for different concentrations of Gd^{+3} was investigated with Wayne Kerr precision component analyzer 6440B. The variation of DC resistivity 'ρ' with temperature over a range of 30^{o}C to 500^{o}C for rare-earth-doped ferrite nano-powders was studied using a two probe setup.

Results And Discussion

2.1 X-ray diffraction

The Rietveld refinement of XRD patterns of nanocrystalline $CoFe_{2-x}Gd_xO_4$ powders recorded at room temperature indicated the existence of a pure spinel phase belonging to the Fd3m space group (Fig. 1). The absence of any extra peak in the diffraction pattern indicated that the rare earth ions were perfectly dissolved into the spinel structure without any traces of hematite formation [21, 25, 30–33]. The substitution of Gd^{+3} (ionic radii 1.02 Å) at the octahedral site replacing a Fe^{+3} without any secondary phase formation can be considered as a prominent feature of the combustion method. The refinement parameters obtained from the refinement of XRD patterns of $CoFe_{2-x}Gd_xO_4$ nanoparticles are presented in Table 1.

Table 1
Rietveld refinement parameters obtained for $CoFe_{2-x}Gd_xO_4$ nanoparticles

Sample $CoFe_{2-x}Gd_xO_4$	χ^2	$R_{Bragg\ factor}$	$R_{F-factor}$
x = 0.0	1.39	14.1	12.3
x = 0.02	1.3	15.3	13.41
x = 0.04	1.33	14.8	12.82
x = 0.05	1.29	14.5	11.0
x = 0.06	1.34	14.9	12.87
x = 0.08	1.36	11.5	8.5
x = 0.1	1.37	12.8	10.2

The samples with concentrations x = 0.04, 0.05, and 0.1showed a drastic increase in lattice parameters and unit cell volume indicating successful substitution of Gd^{+3} at the octahedral site. While the other concentrations (x = 0.06 and 0.08) showed a marginal increase in structural parameters indicating occupancy of Gd^{+3} ions at the interstitial sites. Reduction in intensity of (311) peak indicating an increase in amorphous content in the material [34–41].

2.2 Fourier transforms infrared spectroscopy (FTIR)

The FTIR spectra recorded for $CoFe_{2-x}Gd_xO_4$ nano-crystalline powders are shown in Fig. 3. It is a crucial study that helps in understanding the changes that are caused by the different dopants in the ferrite structure. The FTIR spectra for all the samples showed two major absorption bands in the range 400-650cm^{-1} which are the characteristic features of ferrite material. The absorption band with the lower wavenumbers (400–425 cm^{-1}) is associated with the vibrations of the metal-oxygen bond at the

octahedral site or B-site. The impact of rare earth substitution is predominantly felt on this band as it shows a marginal blue shift in frequency absorption with increasing rare earth concentration [35–43].

2.3 Scanning Electron Microscopy

The morphological study of Gd^{+3} doped cobalt ferrite powders was done using the scanning electron microscope (SEM) instrument. The scanning electron micrographs of $CoFe_{1.98}Gd_{0.02}O_4$ and $CoFe_{1.96}Gd_{0.04}O_4$ are shown in Fig. 4. The SEM micrographs showed a highly agglomerated structure indicating strong magnetic behavior which is a characteristic of transition elements Fe and, Co, and also of inner transition element Gadolinium present in the ferrite samples under investigation [44–47].

Energy dispersive spectra (EDS)

The EDS spectra recorded for $CoFe_2O_4$ and $CoFe_{0.6}Gd_{0.04}O_4$ are shown in **Fig. 5 (a,b)** and the elemental analysis data of three samples is presented in Table 2. All the doped samples showed the presence of Co, Fe, Gd, and O. The weight percentage of Gd in the material was seen to increase with increasing rare earth substitution levels in the cobalt ferrite matrix [44, 45].

Table 2
EDS data of $CoFe_{2-x}Gd_xO_4$ nanoparticles

Sample		Weight %	Atomic %
$CoFe_2O_4$	Co	21.04	15.28
	Fe	41.29	31.64
	O	18.09	48.39
$CoFe_{1.98}Gd_{0.02}O_4$	Co	25.31	20.77
	Fe	46.04	39.87
	Gd	3.23	0.99
	O	11.47	34.68
$CoFe_{1.96}Gd_{0.04}O_4$	Co	29.09	23.25
	Fe	54.79	46.20
	Gd	6.40	1.92
	O	9.73	28.64

2.4 Magnetic properties using vibrating sample magnetometer

The hysteresis loops obtained for Gd^{+3} doped cobalt ferrite samples are shown in Fig. 6. The variation of saturation magnetization (Ms), retentivity (M_R), coercive field (H_C), and anisotropy constant 'K' with Gd^{+3} concentration are shown in **Fig. 7 (a,b,c).** Although the magnetic parameters M_S, M_R, and H_C showed a random variation with increasing Gd^{+3} concentrations, the M_S and M_R were seen to vary inversely to lattice constant and while a direct analogy was observed between H_C and (311) peak height depicting the relation between crystalline nature of the ferrite material. The magnetic environment in cobalt ferrite is administered by Co^{+2}, Fe^{+3} ions. With the spinel geometry, cobaltous ions occupy the tetrahedral site and ferric ions occupy the octahedral site. Generally, the magnetic moment of the material,l in this case,e is expressed in terms of Eq. 1 [45].

Where M is the magnetic moment of the spinel ferrite system, M_B is the magnetic moment of the octahedral site and M_A is the net magnetic moment of the tetrahedral site. Howe, ver with the substitution of a larger rare earth ion Gd^{+3} at the octahedral site, the system experiences an overall lattice expansion and cationic redistribution which changes the overall magnetic moment of the system. This may reduce the strength of super-exchange interaction between the Co^{+2} and Fe^{+3} ions at two cationic sublattice and incomplete ordering of Co^{+2} and Fe^{+3} at the tetrahedral sites and the octahedral sites in the spinel structure

The variations in the magnetic moment can be also caused by changes in canting Yafet-Kittel angle (q_{YK}) due to rare earth substitution. The magnetic moment of the rare earth doped system in this situation is expressed in terms of Eq. 2 [46–50].

2.5 Magnetic susceptibility

The AC susceptibility plots obtained for as prepared $CoFe_{2-x}Gd_xO_4$ are shown in Fig. 8. This measurement proves vital information about the Curie temperature and the type of magnetic domains present in the material. Depending upon the grain size, the domains present in the ferrite are categorized into three categories namely Single domain (SD), multi-domain (MD), and superparamagnetic domain (SP). The MD grains are characterized by the presence of multiple walls within the grain. If the grain size is comparable to that of the wall thickness then these grains are termed as single domains. Superparamagnetic behavior is predominantly seen in particles with dimensions < 10 nm. Here, the magnitude of thermal energy is comparable to that of magnetic anisotropy energy.

It can be seen from Fig. 8 that there is a gradual increase in normalized AC susceptibility followed by a steep rise creating a peak at high temperature before a sharp fall in the vicinity of the Curie temperature. This indicates that the as prepared samples contain a large section of single domain and a good number of multi-domain grains as well. The values of curie temperature for all the samples were in the range of 525^{o}C to 575^{o}C [51–53].

2.6 DC Resistivity

The plots of temperature-dependent variation of DC resistivity (ρ) over a range of 300K to 773K for rare earth doped cobalt ferrite samples are presented in Fig. 9. The rare earth doped ferrite powders showed an increase in resistivity with increasing temperature initially till a resistivity maxima of the order 10^7 Ω-cm in the temperature range of 473K to 523K. These high resistivity values are the attributes of the removal of moisture present in the interstitial sites that facilitates the conduction mechanism. The high resistivity of the order 10^7 Ω-cm can be attributed to the smaller grain size and the large number of grain boundaries available in the nanomaterials. These grain boundaries are characterized by their insulating nature and play a very important role in increasing the material resistivity [54–57]. The rare-earth ions (Gd^{+3}) being a larger ion occupies the spacious octahedral site replacing Fe^{+3} ions which are generally known as a source of charge carriers. Hence this reduction in Fe^{+3} ions also causes the depletion of charge carriers [58–60]. The larger ionic radii of Gd^{+3} ions also alter the electron hopping mechanism adversely by causing lattice expansion. This increases the separation between Co^{+2} and Fe^{+3} ions reducing the electronic exchange [61, 62].

2.7 Dielectric constant variation with frequency

The plot of frequency dependence of dielectric constant is shown in Fig. 10 (a) and the values of dielectric constant as at 20Hz for different Gd^{+3} concentrations are shown in Fig. 10 (b)

The Dielectric constant ‘ε’ was seen to decrease with the increasing frequency of the applied electric field and was seen to remain constant beyond a critical value of frequency. The increasing Gd^{3+} occupancy at the B site replacing a smaller ion Fe^{3+} was also seen to affect the variation of the dielectric constant [63–66]. The Dielectric behavior of cobalt ferrite nanomaterials material is administered by the electronic exchange between metal ions and primarily dominated by the Fe^{3+}/Co^{2+} ions. The doping of rare-earth ions Gd^{3+} ions alters the structural parameters such as cell volume, density, lattice constant etc. and also decrease Fe^{+3} ion concentrations at the octahedral site. As a result, the electron hopping between Fe^{3+} and Co^{2+} ions gets affected adversely [67–70]. The dielectric constant profile showed a steep reduction in magnitude to a lower value with an increase in frequency in the lower frequency region attain a constant low value that remains constant over higher frequency values of the applied field. This variation in dielectric properties can be explained using the space charge polarization phenomenon. An ideal dielectric material is comprised of highly conducting grains. These grains are bounded by nonconducting grain boundaries. When the electric field is applied, a potential drop occurs at the grain boundaries as a result of the accumulation of space charge in this region. The influence of the grain boundaries is observed distinctly over the lower frequency range. Beyond a certain value of applied field frequency, the electronic transfer between the metal ions starts lagging behind the rate of variation in the frequency of an applied electric field. This results in uniform lower magnitudes of dielectric constants[68–70].

2.8 Dielectric loss variation with frequency

The variation of dielectric loss versus frequency for varying Gd^{3+} concentrations is presented in Fig. 11a. While the loss values for different Gd^{+3} concentrationS in cobalt ferrite samples at 20Hz are presented in

Fig. 11b.

It can be seen that for nanoparticle samples dielectric loss decreases with increasing frequency of applied electric field and attains a low constant value beyond a critical frequency. At lower frequencies, the dielectric curve is seen to exhibit broad peaks in the neighborhood of 100Hz. The profile depicted in Fig. 11b shows an approximately inverse behavior of dielectric loss to that of dielectric constant at 10Hz. The variation in the dielectric loss with increasing Gd^{3+} concentrations at low frequencies could be due to hindrance in the electronic exchange between Co^{+2}/Fe^{+3} and Fe^{+2}/Fe^{+3} [69–75]. At higher frequencies, the dielectric loss decreases drastically which may allow these materials to find their applications in high-frequency devices [76–79].

Conclusion

The ultrafine powders of Gd^{+3}doped cobalt ferrite with composition $CoFe_{2-x}Gd_xO_4$ (x=0.0, 0.02,0.04,0.05, 0.06, 0.08, 0.1) with cubic spinel structure and crystallite size ranging between 21 nm to 41 nm were prepared successfully using combustion route. The structural parameters such as lattice constant '*a*', X-density 'D_X', and unit cell volume were altered drastically due to Gd^{+3} substitution at the octahedral site. The particle agglomerates seen in the SEM images indicated a strong magnetic behavior. The EDS spectra showed the presence of Co, Fe, and Gd in desired quantities without any impurities. The A.C. susceptibility measurements indicated the presence of both single-domain and multidomain particles in all the samples. The changes observed in magnetic properties were attributed to cationic redistribution, lattice expansion, and alterations in magnetic ordering due to Gd^{+3} substitution.

The DC resistivity profile for all the samples showed high room-temperature resistivity of the order 10^7W-cm. The dielectric constant values were also seen to be administered by the concentrations of Gd^{+3} at the octahedral site. The dielectric constant variation was explained using the space charge polarization phenomenon. The variation in the dielectric loss with increasing Gd^{3+} concentrations at low frequencies was attributed to hindrance in the electronic exchange between Fe^{+2}/Fe^{+3} and Co^{+2}/Fe^{+3}. At higher frequencies, all the samples were seen to exhibit low losses making them a potential candidate for high energy applications.

Declarations

We, the authors of this manuscript entitled “Influence of B-site Gd+3 substitution on various properties of Co-ferrite nanoparticles” declare that, This article is original And has been written by the stated authors who are all aware of its content and approve its submission. The article has not been published previously is not under consideration for publication elsewhere. We also declare that there exist no conflict of interest.

References

1. S. Thakur, S.C. Katyal, M. Singh, Structural and magnetic properties of nano nickel-zinc ferrite synthesized by reverse micelle technique. J. Magn. Magn. Mater. **321**, 1–7 (2009)
2. M. Sertkol, Y. Köseoğlu, A. Baykal, H. Kavas, M.S. Toprak, Syn- thesis and magnetic characterization of $Zn_{0.7}Ni_{0.3}Fe_2O_4$ nanopar- ticles via microwave-assisted combustion route. J. Magn. Magn. Mater. **322**, 866–871 (2010)
3. M.H. Abdellatif, G.M.E. Komy, A.A. Azab, Magnetic characterization of rare earth doped spinel ferrite. J. Magn. Magn. Mater. **442**, 445–452 (2017)
4. F. Nirav Joshi, Luís, H.S. da Silva, F.M. Jadhav, P.H. Shimizu, Jean-ClaudeM.'Peko Suman, Marcelo Ornaghi Orlandi, Jeong Gil Seo, Valmor R Mastelaro, Osvaldo N Oliveira Jr, Yolk-shelled $ZnCo_2O_4$ microspheres: Surface properties and gas sensing application. Sens. Actuators B **257**, 906–915 (2018)
5. F. Nirav Joshi, Luis, H. Silva, M.'Peko Jadhav, Jean-Claude, B.B.M. Torres, K. Aguir, R. Valmor, N. Mastelaro, Osvaldo, Oliveira, One-step approach for preparing ozone gas sensors based on hierarchical NiCo2O4 structures. RSC Adv. **6**, 92655–92662 (2016)
6. F. Nirav Joshi, Luís, H.S. da Silva, F.M. Jadhav, P.H. Shimizu, M.'Peko Suman, Jean-Claude, Marcelo Ornaghi Orlandi, Jeong Gil Seo, R. Valmor, N. Mastelaro, Osvaldo, Oliveira Jr., Yolk-shelled ZnCo2O4 microspheres: Surface properties and gas sensing application, Sensors and Actuators B: Chemical, **257**, 906–915, (2018)
7. N. Joshi, T. Hayasaka, Y. Liu, H. Liu, N. Osvaldo, L. Oliveira Jr., Lin, A review on chemiresistive room temperature gas sensors based on metal oxide nanostructures, graphene and 2D transition metal dichalcogenides. Microchim. Acta **185**(4), 213 (2018)
8. V.K. Ritu Malik, N. Tomer, T. Joshi, L. Dankwort, L. Lin, Kienle, *Au–TiO2-Loaded Cubic g-C3N4 Nanohybrids for Photocatalytic and Volatile Organic Amine Sensing Applications*, 10 (ACS applied materials & interfaces, 2018), 40, 34087–34097
9. A. Singh, A. Kumar, A. Kumar, S. Samanta, N. Joshi, V. Balouria, A.K. Debnath, R. Prasad, Z. Salmi, M.M. Chehimi, D.K. Aswal, S.K. Gupta, Bending stress induced improved chemiresistive gas sensing characteristics of flexible cobalt-phthalocyanine thin films, Applied Physics Letters,102,132107, (2013)
10. B. Skolyszewska, W. Tokarz, K. Przybylski, Z. Kakol, Preparation and magnetic properties of Mg-Zn and Mn-Zn ferrites. Physica C **38**, 290 (2003)
11. H. Ibrahim Sharifi, S. Shokrollahi, Amiri, Ferrite-based magnetic nanofluids used in hyperthermia applications. J. Magn. Magn. Mater. **324**, 903–915 (2012)
12. Stephen, Blundell, *Magnetism in Condensed Matter* (Oxford University Press, Oxford, 2001)
13. S. Mahalakshmi, M. Srinivasa, S. Nithiyanantham, Magnetic studies of nickel ferrite doped with rare earth ions. Russ. J. Phys. Chem. **87**, 1938 (2013)
14. A.A. Sattar, A.H. Wafik, K.M. El-Shokroty, M.M. El-Tabby, Phys. State Solid A **171**, 563 (1999)

15. M.P. Ghosh, S. Mukherjee, J. Magn. Magn. Mater. **489**, 165320 (2019)
16. H. Yoon, J.S. Lee, J.H. Min, J.H. Wu, Y.K. Kim, Nanosci. Res. Lett. **8**, 530 (2013)
17. Y. Shifeng, E. WeiLing, Zhou, Rapid synthesis of Mn0.65Zn0.35 Fe2O4/SiO2 homogeneous nano-composites by modified sol-gel auto-combustion method,Journal Crystal Growth, 226–233 (2004)
18. C. Scherer, A.M. Figueiredo Neto, Ferrofluids: properties and applications. Braz. J. Phys. **35**(3), 718–727 (2005)
19. C.C. Berry, "Progress in functionalization of magnetic nanoparticles for applications in biomedicine," Journal of Physics D, vol. 42, no. 22, Article ID 224003, 9 pages, 2009
20. H. Tan, J.M. Xue, B. Shuter, X. Li, J. Wang, Synthesis of PEOlated Fe3 O4 @SiO2 nanoparticles via bioinspired silification for magnetic resonance imaging. Advanced Functional Materi- als **20**(5), 722–731 (2010)
21. P. Pranav, R.B. Naik, Tangsali, Enduring effect of rare earth (Nd^{3+}) doping, and γ- radiation on electrical properties of nanoparticle manganese zinc ferrite. J. Alloy. Compd. **723**, 266–275 (2017)
22. G. Baldi, D. Bonacchi, C. Innocenti, G. Lorenzi, C. Sangre- gorio, Cobalt ferrite nanoparticles: the control of the particle size and surface state and their effects on magnetic properties. J. Magn. Magn. Mater. **311**(1), 10–16 (2007)
23. G. Baldi, D. Bonacchi, M.C. Franchini et al., Synthesis and coating of cobalt ferrite nanoparticles: a first step toward the obtainment of new magnetic nanocarriers. Langmuir **23**(7), 4026–4028 (2007)
24. A.R. Alam Abedini, Daud, Muhammad Azmi Abdul Hamid, Norinsan Kamil Othman, Radiolytic formation of Fe3O4 nanoparticles: influence of radiation dose on the structure and magnetic properties, (3) 1–8. (2014)
25. P. Pranav, R.B. Naik, S.S. Tangsali, S.M. Meena, Yusuf, Influence of rare earth (Nd^{3+}) doping on structural and magnetic properties of nanocrystalline manganese-zinc ferrite. Mater. Chem. Phys. **191**, 215–224 (2017)
26. P.S. Bharat Kataria, U. Solanki, M. Khachar, A. Vagadia, M.J. Ravalia, P. Keshvani, D. Trivedi, V. Venkateshwarlu, K. Ganesan, N.A. Asokan, D.G. Shah, Kuberkar, Role of strain and microstructure in chemical solution deposited $La_{0.7}Pb_{0.3}MnO_3$ manganite films: thickness-dependent swift heavy ions irradiation studies. Rad. Phys. Chem. **85**, 173–178 (2013)
27. M. Deepak Kumar, A. D'souza, M. Chatim, V. Naik, P.P. Naik, R.B. Tangsali, Effect of Rare-earth doping on Magnetic and Electrical Transport Properties of Nanoparticle Mn Zn Ferrite. Adv. Sci. Lett. **22**, 773–779 (2016)
28. S. Nidhi Tendulkar, V. Patil, P.P. Kuncalienkar, M. Naik, S. Kundaikar, Keluskar, Study of Structural and Magnetic Properties of $Mn_{0.8}Zn_{0.2}Fe_2O_4$ Nanoparticles, Advanced Engineering Technology and Application, 5, No. 1, 19–22 (2016)
29. N.Hanh, O.K.Quy, N.P.Thuy, L.D.Tung, L..Spinu, Synthesis of cobalt ferrite nanocrystallites by the forced hydrolysis method and investigation of their magnetic properties. Phys. B **327**, 382–384 (2003)

30. L. Xuebo Caol, Gu, Spindly cobalt ferrite nanocrystals: preparation, characterization and magnetic properties, Nanotechnology16 180–185 (2005)
31. Z. Cvejic, B. Antic, A. Kremenovic, S. Rakic, G.F. Goya, H.R. Rechenberg, C. Jovalekic, V. Spasojevic, Influence of heavy rare earth ions substitution on microstructure and magnetism of nanocrystalline magnetite. J. Alloys Compd. **472**, 571–575 (2009)
32. S.M. Patange, S.E. Shirsath, G.S. Jangam, K.S. Lohar, S.S. Jadhav, K.M. Jadhav, Rietveld structure refinement, cation distribution and magnetic properties of Al^{3+} substituted $NiFe_2O_4$ nanoparticles. J. Appl. Phys. **109**, 053909 (2011)
33. N. Menon, S.R. Nagel, Evidence for a divergent suscepti- bility at the glass transition. Phys. Rev. Lett. **74**(7), 1230–1233 (1995)
34. G.A. Sawatzky, F. van der Woude, A.H. Morrish, Mo¨ssbauer study of several ferrimagnetic spinels. Phys. Rev. **187**(2), 747–757 (1969)
35. M.A. Amer, Structural and magnetic studies of the $Co_{1+x}Ti_xFe_{2(1-x)}O_4$ ferrites. J. Magn. Magn. Mater. **426**, 771–778 (2017)
36. M.A. Amer, A. Matsuda, G. Kawamura, R. El-Shater, T. Meaz, F. Fakhry, Characterization and structural and magnetic studies of as-synthesized $Fe^{2+}Cr_xFe_{(2-x)}O_4$ nanoparticles. J. Magn. Magn. Mater. **439**, 373–383 (2017)
37. E.H. El-Ghazzawy, M.A. Amer, Structural, Elastic and magnetic studies of the as-synthesized Co1 – xSrxFe2O4 nanoparticles. J. Alloy. Compd. **690**, 293–303 (2017)
38. Y.G. Zhang, Magnetic Materials, Chengdu, Pekin, 1988 (Chap. 1)
39. S.R. Naik, A.V. Salker, Change in the magnetostructural properties of rare-earth-doped cobalt ferrites relative to the magnetic anisotropy. Journal of Material Chemistry **22**, 2740 (2012)
40. L. Zhao, H. Yang, X. Zhao, L. Yu, Y. Cui, S. Feng, Magnetic properties of CoFe2O4 ferrite doped with rare-earth ion, Material Letters 60 1–6, (2006)
41. B.V. Ch Srinivas, A. Tirupanyam, V. Satish, D.L. Seshubai, O.F. Sas- try, Caltun, Effect of Ni2 + substitution on structural and mag- netic properties of Ni–Zn ferrite nanoparticles. J. Magn. Magn. Mater. **382**, 15–19 (2015)
42. 17. Ch Srinivas, B.V. Tirupanyam, S.S. Meena, S.M. Yusuf, C.S. Babu, K.S. Ramakrishna, D.M. Potukuchi, D.L. Sastry, Structural and magnetic characterization of co-precipitated NixZn1–xFe2O4 ferrite nanoparticles. J. Magn. Magn. Mater. 407, 135–141 (2016)
43. F.-X. Cheng, J.-T. Jia, Z.-G. Xu, B. Zhou, C.-S. Liao et al., Microstructure, magnetic, and magneto-optical properties of chemical synthesized Co–RE (RE = Ho,†Er,†Tm,†Yb,†Lu) ferrite nanocrystalline films. J. Appl. Phys. **86**, 2727–2732 (1999)
44. K.S. Rane, V.M.S. Verenkar, Synthesis of ferrite grade γ-Fe2O3. Bull. Mater. Sci. **24**, 39–45 (2001)
45. 20R.A. Porob, S.Z. Khan, S.C. Mojumdar, V.M.S. Veren- kar, Synthesis, TG, DSC, and infrared spectral study of NiMn2(C4H4O4)3·6N2H4-a precursor for NiMn2O4 nanoparticles. J. Therm. Anal. Calorim. **86**, 605–608 (2006)

46. S. Anjali Bishnoi, Kumar, Nirav Joshi Wide-Angle X-ray Diffraction (WXRD): Technique for Characterization of Nanomaterials and Polymer Nanocomposites. Microscopy Methods in Nanomaterials Characterization **1**, 313–337 (2017)
47. A. Baykal, F. Genç, A.Z. Elmal, S. Geokçe, M. Sertkol, H. Seozeri, MnCrxFe2 – xO4 Nanoparticles: Magnetic and Microwave Absorption Properties. J. Inorg. Organomet. Polym Mater. **26**, 134–141 (2016)
48. H. Shenker, Magnetic anisotropy of cobalt ferrite (Co1.01 Fe2.00O3.62) and nickel cobalt ferrite (Ni0.72Fe0.20Co0.08Fe2O4). Phys. Rev. **107**(5), 1246–1249 (1957)
49. M.B. Morales, M.H. Phan, S. Pal, N.A. Frey, H. Srikanth, "Particle blocking and carrier fluid freezing effects on the magnetic properties of Fe3O4 -based ferrofluids," Journal of Applied Physics, vol. 105, no. 7, Article ID 07B511, 3 pages, 2009
50. G. Baldi, D. Bonacchi, C. Innocenti, G. Lorenzi, C. Sangre- gorio, Cobalt ferrite nanoparticles: the control of the particle size and surface state and their effects on magnetic properties. J. Magn. Magn. Mater. **311**(1), 10–16 (2007)
51. N.D. Chaudhari, R.C. Kambale, D.N. Bhosale, S.S. Suryavanshi, S.R. Sawant, Thermal hysteresis and domain states in Ni-Zn fer- rites synthesized by oxalate precursor method. J. Magn. Magn. Mater. **322**, 1999–2005 (2010)
52. O.A. Li, C.-R. Lin, H.-Y. Chen, H.-S. Hsu, K.-Y. Shih, I.S. Edelman, K.-W. Wu, Y.-T. Tseng, S.G. Ovchinnikov, J.-S. Lee, Size dependent magnetic and magneto-optical properties of Ni0.2Zn0.8Fe2O4 nanoparticles. J. Magn. Magn. Mater. 408, 206–212 (2016)
53. V. Grimal, D. Autissier, L. Longuet, H. Pascard, M. Gervais, Iron, nickel and zinc stoichiometric influences on the dynamic magneto-elastic properties of spinel ferrites. J. Eur. Ceram. Soc. **26**, 3687–3693 (2006)
54. P.P. Naik, R.B. Tangsali, B. Sonaye, S. Sugur, Radiation stimulated permanent alterations in structural and electrical properties of core-shell Mn-Zn ferrite nanoparticles. J. Nano Res. Vol **24**, 194–202, (2013) pp
55. P. Pranav, R.B. Naik, B. Tangsali, S. Sonaye, Sugur, Sustained augmentation in electrical properties of MnxZn1-xFe2O4 nanoparticles provoked by high energy gamma radiation. Journal of Nanotechnology and Advanced Materials **3**(1), 1–7 (2015)
56. V. Manisha, D. Rane, A.K. Bahadur, Nigam, C.M. Srivastava, Mössbauer and FT-IR studies on non-stoichiometric barium hexaferrites. J. Magn. Magn. Mater. **192**, 288–296 (1999)
57. P. Pranav, R.B. Naik, Tangsali, Enduring Effect of Rare Earth (Nd^{+3}) Doping and, γ- Radiation on Electrical properties of Nanoparticle Manganese Zinc Ferrite. J. Alloy. Compd. **723**, 266–275 (2017)
58. M. Asif Iqbal, M.U. Islam, I. Ali, M.A. Khan, I. Sadiq, I. Ali, High-frequency dielectric properties of Eu + 3-substituted Li–Mg ferrites synthesized by sol-gel auto-combustion method. J. Alloy. Compd. **586**, 404–410, (2014)
59. B. Chandra Babu, N.V. Jayaprakash., S. B, Buddhudu, Structural, thermal and dielectric properties of lithium zinc silicate ceramic powders by sol-gel method. Ferro Electrics letter **38**, 114–127 (2011)

60. N. Rezlescu, E. Rezlescu, Dielectric properties of copper containing ferrites. Physics Status Solidi A. **23**, 575–582 (1974)
61. I.H. Gul, A. Maqsood, M. Naeem, M. Naeem Ashiq, Optical, magnetic and electrical investigation of cobalt ferrite nanoparticles synthesized by co-precipitation route. J. Alloys Compd. **507**, 201–206 (2010)
62. M.T. Farid, I. Ahmad, S. Aman, Characterization of nickel-based spinel ferrites with small substitution of praseodymium. Journal of Chemical Society of Pakistan **35**, 793–799 (2013)
63. V.D. Mote, Y. Purushottam, B.N. Dole, Williamson-Hall analysis in estimation of lattice strain in nanometer-sized ZnO particles. J. Theor. Appl. Phys. **6**, 2251–7235 (2012)
64. C. Venkataraju, Effect of nickel on the structural properties of Mn Zn ferrite nanoparticles. Appl. Phys. Res. **1**(1), 41–45 (2009)
65. L. Zhao, H. Yang, X. Zhao, L. Yu, Y. Cui, S. Feng, Magnetic properties of CoFe2O4 ferrite doped with rare earth ion, Mater. Lett. 60,1–6, (2006)
66. M.M. Haque, M. Huq, M.A. Hakim, Effect of Cu for Mn on the magnetic properties of Mn-Zn ferrites. Indian J. Phys. **78A**(3), 397–400 (2004)
67. M.M. Emad, M.M. Ewais, A. Hessien, Abdel-Hady. El-Geassy, In-situ synthesis of magnetic Mn-Zn ferrite ceramic object by solid state reaction. J. Aust. Ceram. Soc. **44**(1), 57–62 (2008)
68. K. Rama Krishna, K. Vijaya Kumar, D. Ravinder, Structural and electrical conductivity studies in nickel-zinc ferrite. Adv. Mater. Phys. Chem. **2**, 185–191 (2012)
69. M.F. Sarac, Magnetic, Structural, and Optical Properties of Gadolinium-Substituted $Co_{0.5}Ni_{0.5}Fe_2O_4$ Spinel Ferrite Nanostructures, Journal of Superconductivity and Novel Magnetism, doi.org/10.1007/s10948-019-05359-3
70. C. Murugesan, G. Chandrasekaran, Impact of Gd^{3+} substitution on the structural, magnetic and electrical properties of cobalt ferrite nanoparticles. RSC Adv. **5**, 73714–73725 (2015)
71. J.G. Kang, B.K. Min, Y. Sohn, Synthesis and characterization of $Gd(OH)_3$ and Gd_2O_3 nanorods. Ceram. Int. **41**, 1243–1248 (2015)
72. M.T. Farid, I. Ahmad, S. Aman, M. Kanwal, G. Murtaza, I. Ali, I. Ahmad, M. Iashfaq, Structural, electrical and dielectric behavior of NixCo1-xNdyFe2-yO4 nano ferrites synthesized by Sol-Gel Method. Digest Journal of Nanomaterials and Biostructures **10**(1), 265–275 (2015)
73. G. Kumar, J. Shah, R.K. Kotnala, P. Dhiman, R. Rani, V.P. Singh, G. Garg, S.E. Shirsath, K.M. Batoo, M. Singh, Self-ignited synthesis of Mg–Gd–Mn nano ferrites and impact of cation distribution on the dielectric properties. Ceram. Int. **40**(9), 14509–14516, (2014)
74. K.W. Wagner, Dissipation of energy under AC. American Physics **40**, 317 (1973)
75. S. Snehal, P.P. Hasolkar, Naik, Effect of Gd + 3 doping on structural, Magnetic and electrical properties of Mn0.5Co0.5Fe2-xGdxO4nano-particles prepared using combustion synthesis. J. Alloy. Compd. **823**, 153605 (2020)

76. L. Ajroudi, N. Mliki, L. Bessais, V. Madigou, S. Villain, Ch. Leroux, Magnetic, electric and thermal properties of cobalt ferrite nanoparticles. Mater. Res. Bull. **59**, 49–58 (2014)
77. N.J. Joshi, G.S. Grewal, V. Shrinet, T.P. Govindan, A. Pratap, Synthesis and dielectric behavior of nano-scale barium titanate. IEEE dielectrics &Electrical Insulations **19**, 83–90 (2012)
78. N.J. Joshi, G.S. Grewal, V. Shrinet, A. Pratap, N.J. Buch, Synthesis and characterization of nano-barium titanate prepared by hydrothermal process. Integrated Ferroelectrics **115**, 142–148, (2010)
79. A. Pratap, N.J. Joshi, P.B. Rakshit, G.S. Grewal, V. Shrinet, Dielectric behavior of nano barium titanate filled polymeric composites, International Journal of Modern Physics: Conference Series,22,1–10, (2013)

Figures

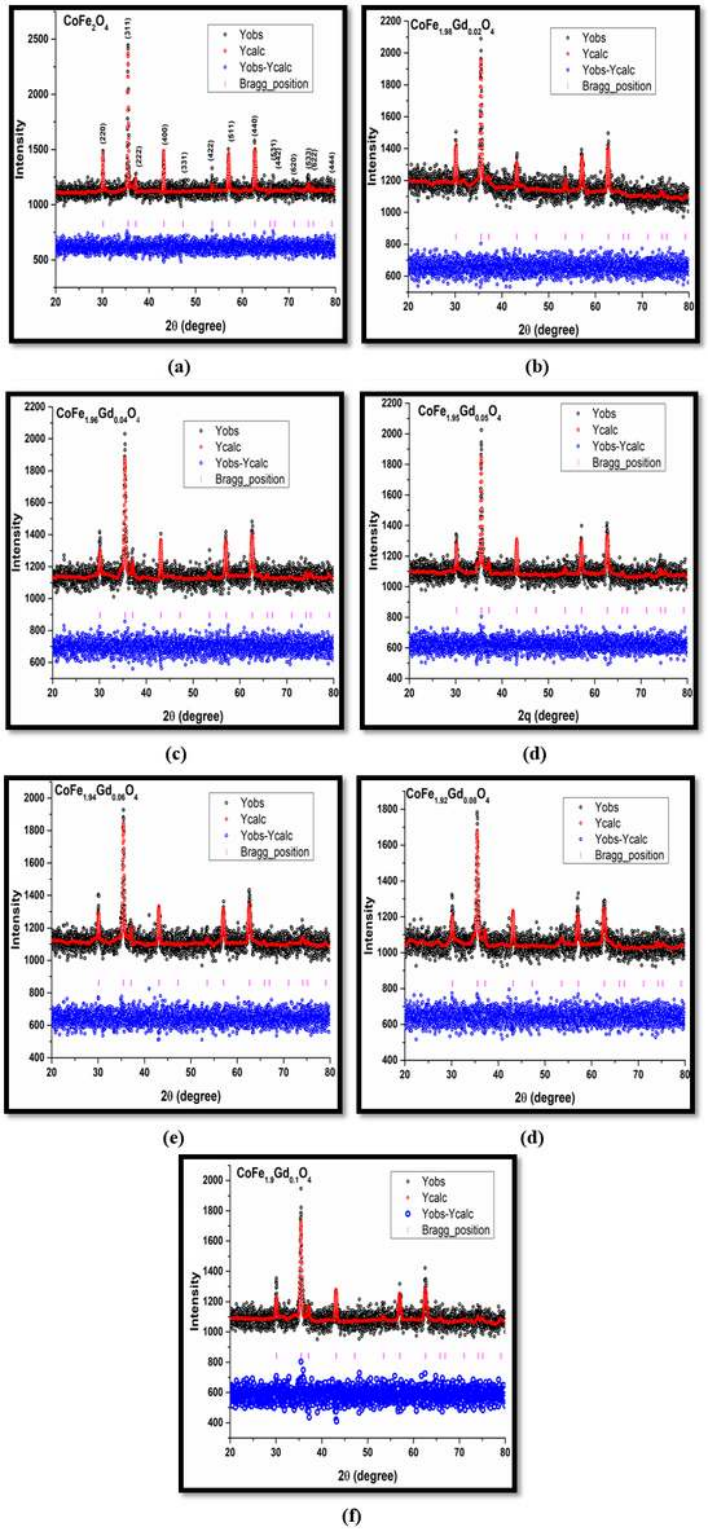

Figure 1

Rietveld refinement of X-ray diffraction pattern CoFe2-xGdxO4 nanoparticles.

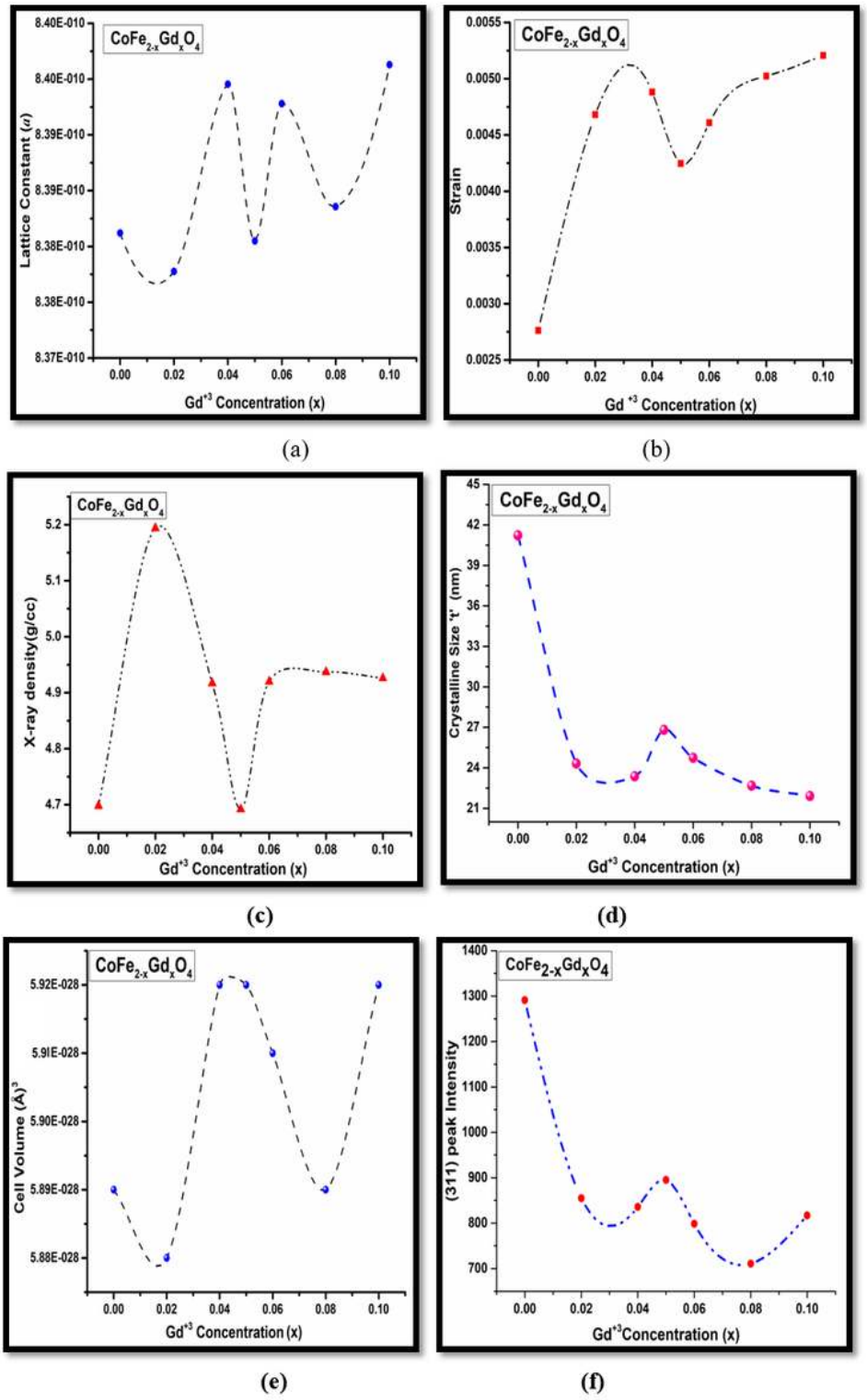

Figure 2

Variation in structural parameters such as a) Lattice constant ‘a’, b) Lattice strain, c) X-ray density ‘DX’, d) Crystallite size ‘t’, and e) Cell volume f) (311) peak intensity with Gd+3 concentration

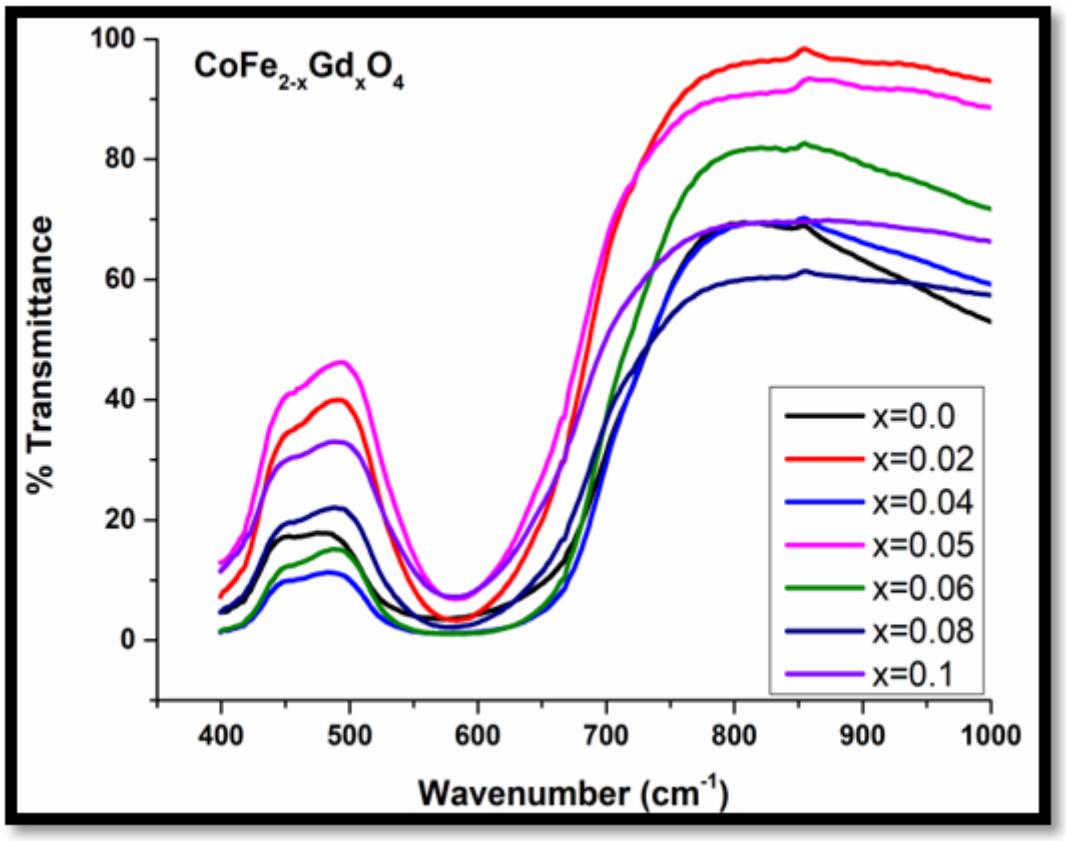

Figure 3

Fourier transform infrared spectra of CoFe2-xGdxO4 nanoparticles

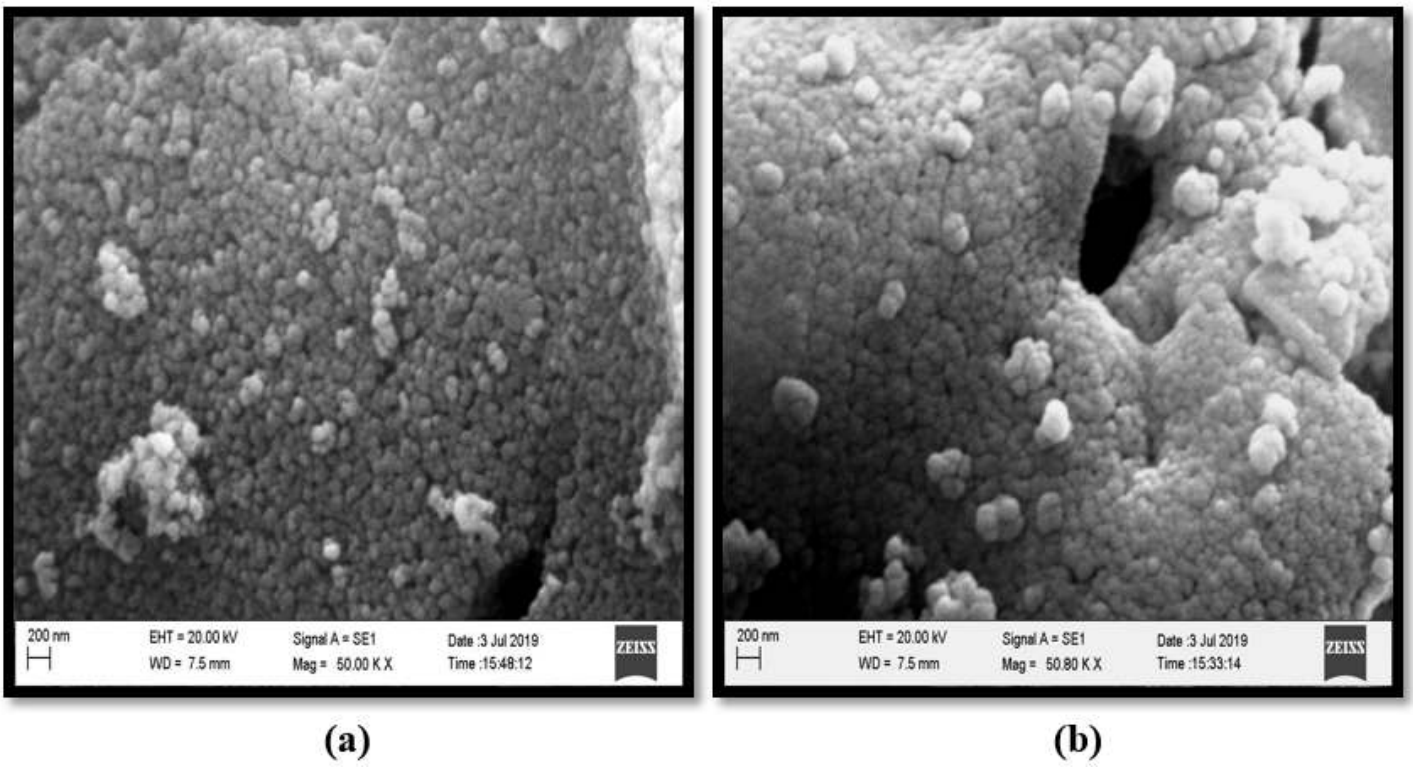

Figure 4

Scanning Electron micrographs of CoFe1.98Gd0.02O4 and CoFe1.96Gd0.04O4

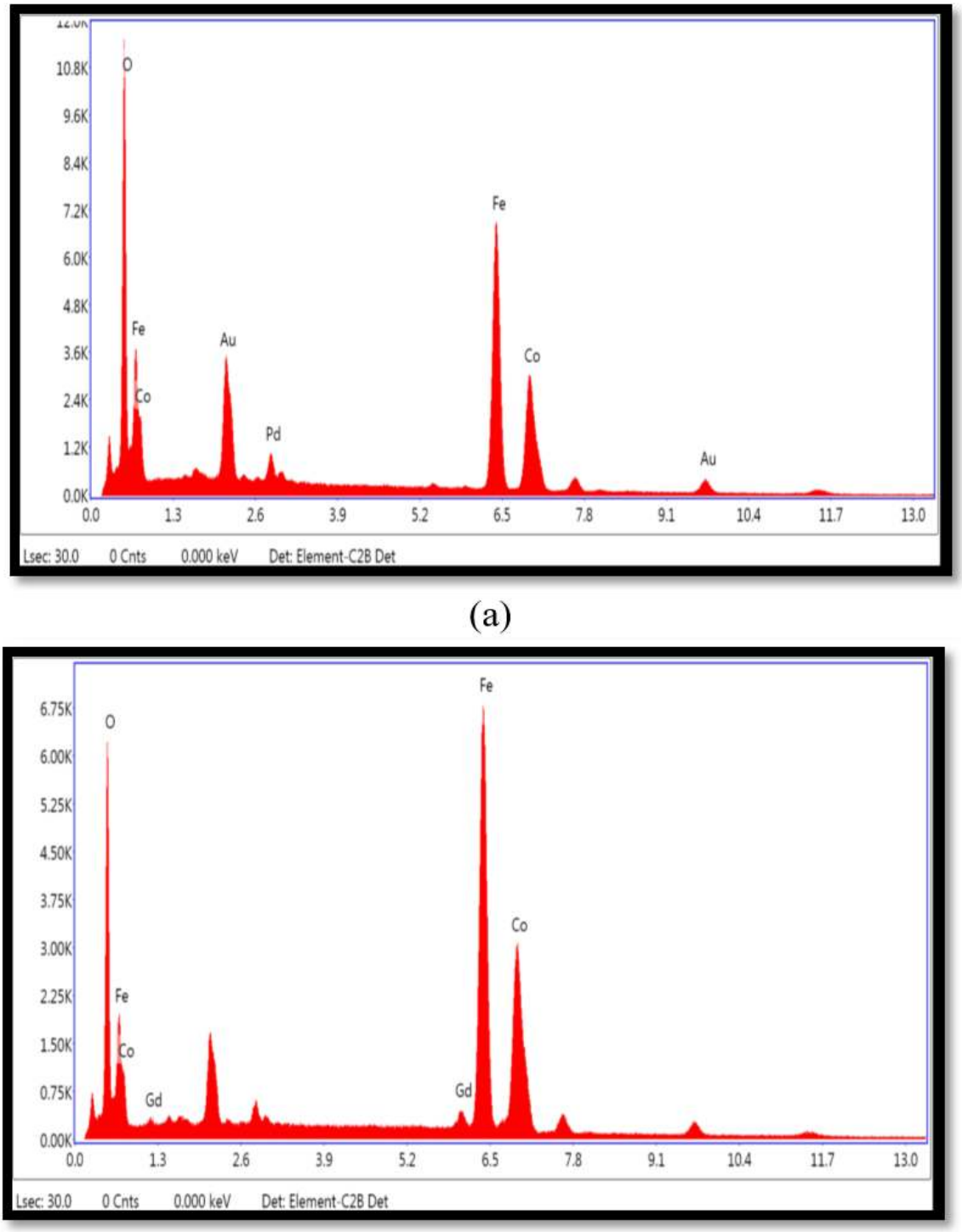

Figure 5

Energy dispersive spectrum of (a) CoFe2O4 (b) CoFe1.96Gd0.04O4

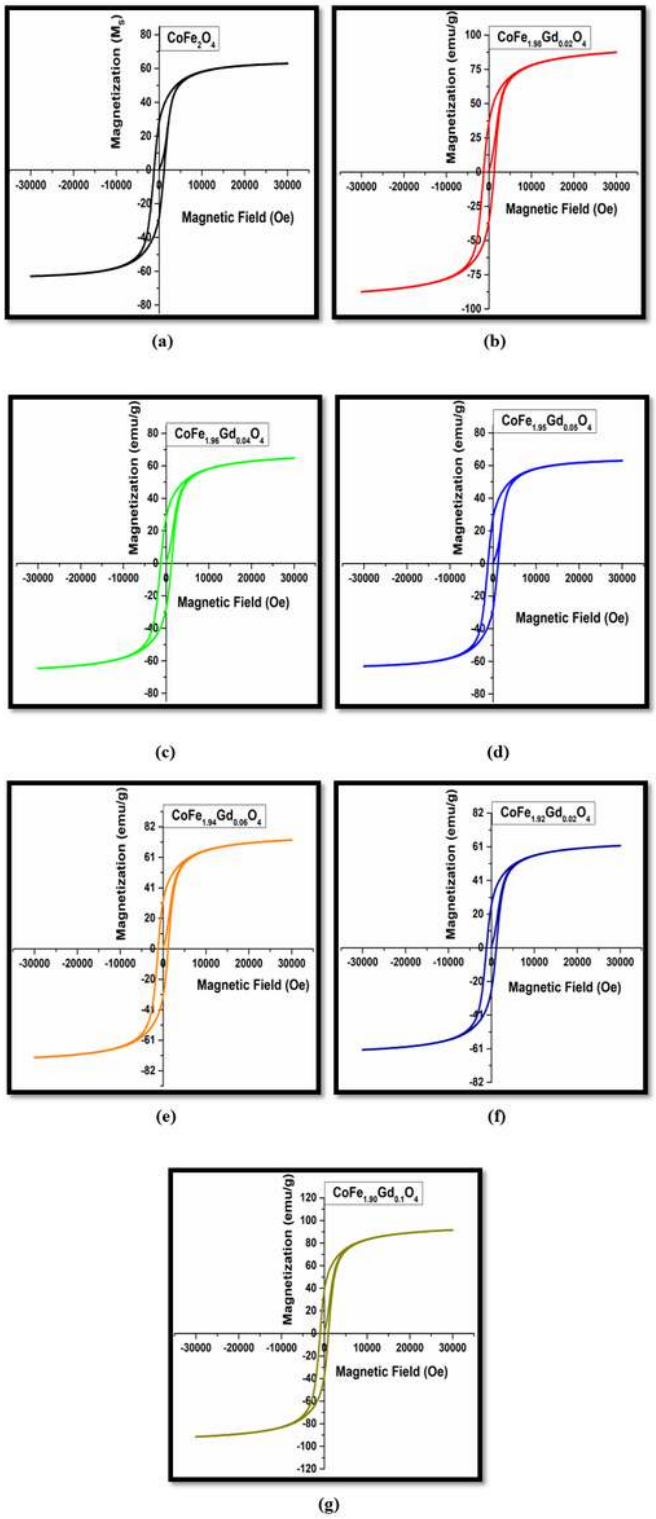

Figure 6

Magnetic hysteresis loops of CoFe2-xGdxO4 nanoparticles

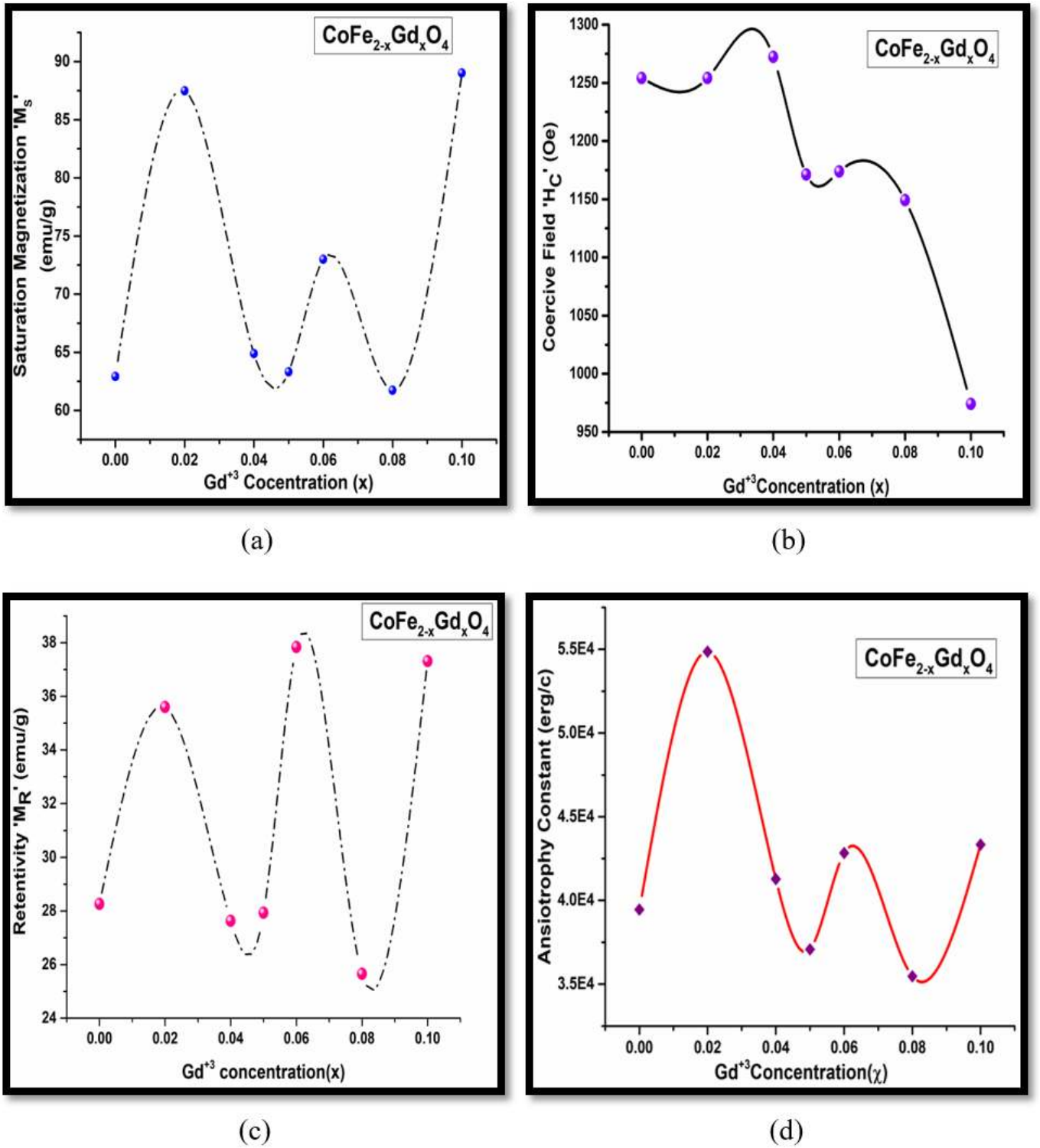

Figure 7

Magnetic parameters of CoFe2-xGdxO4 nanoparticles

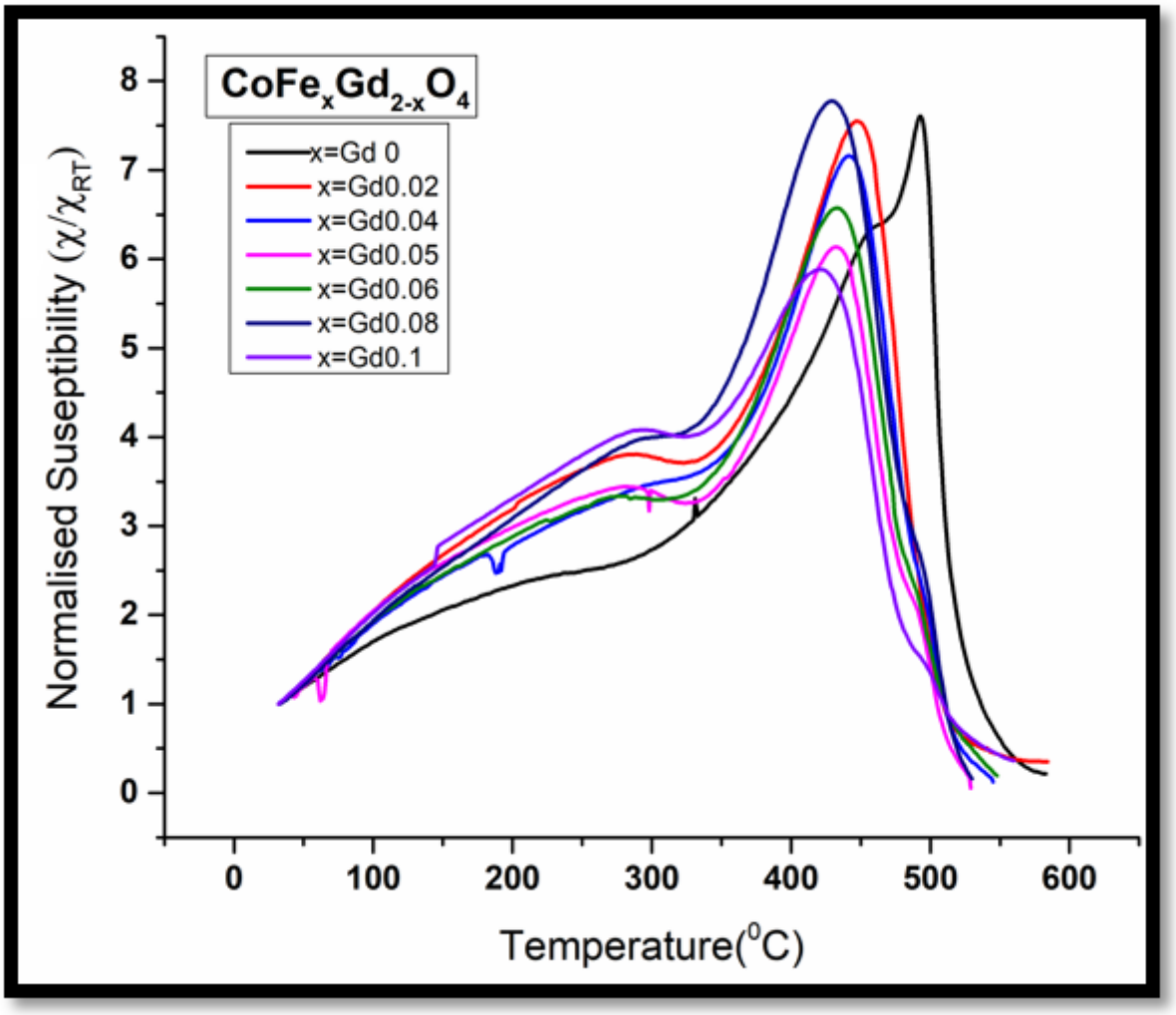

Figure 8

The normalized AC susceptibility of CoFexGd1-xO4

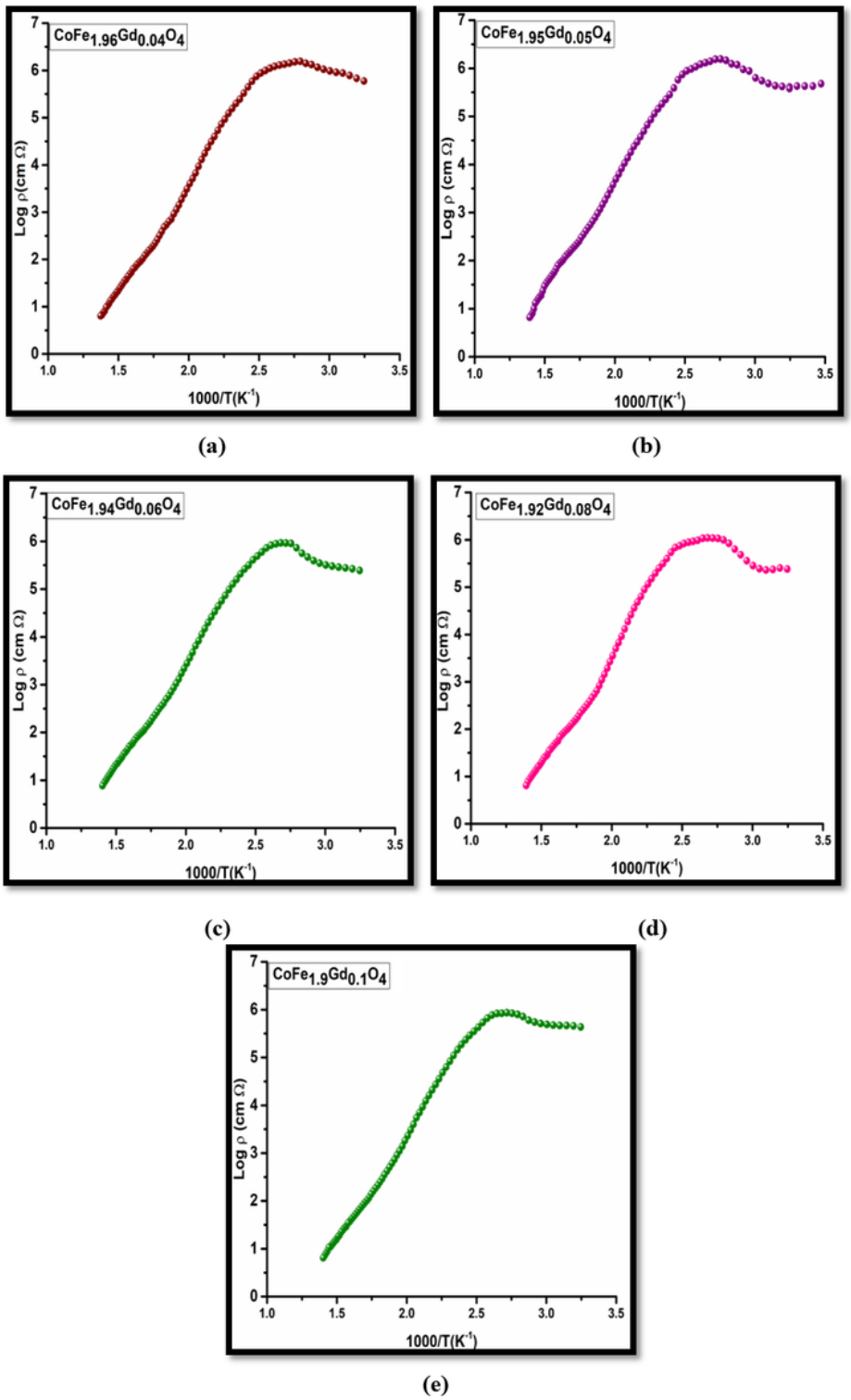

Figure 9

DC Resistivity variations with temperature for CoFe2-xGdxO4 nanoparticles

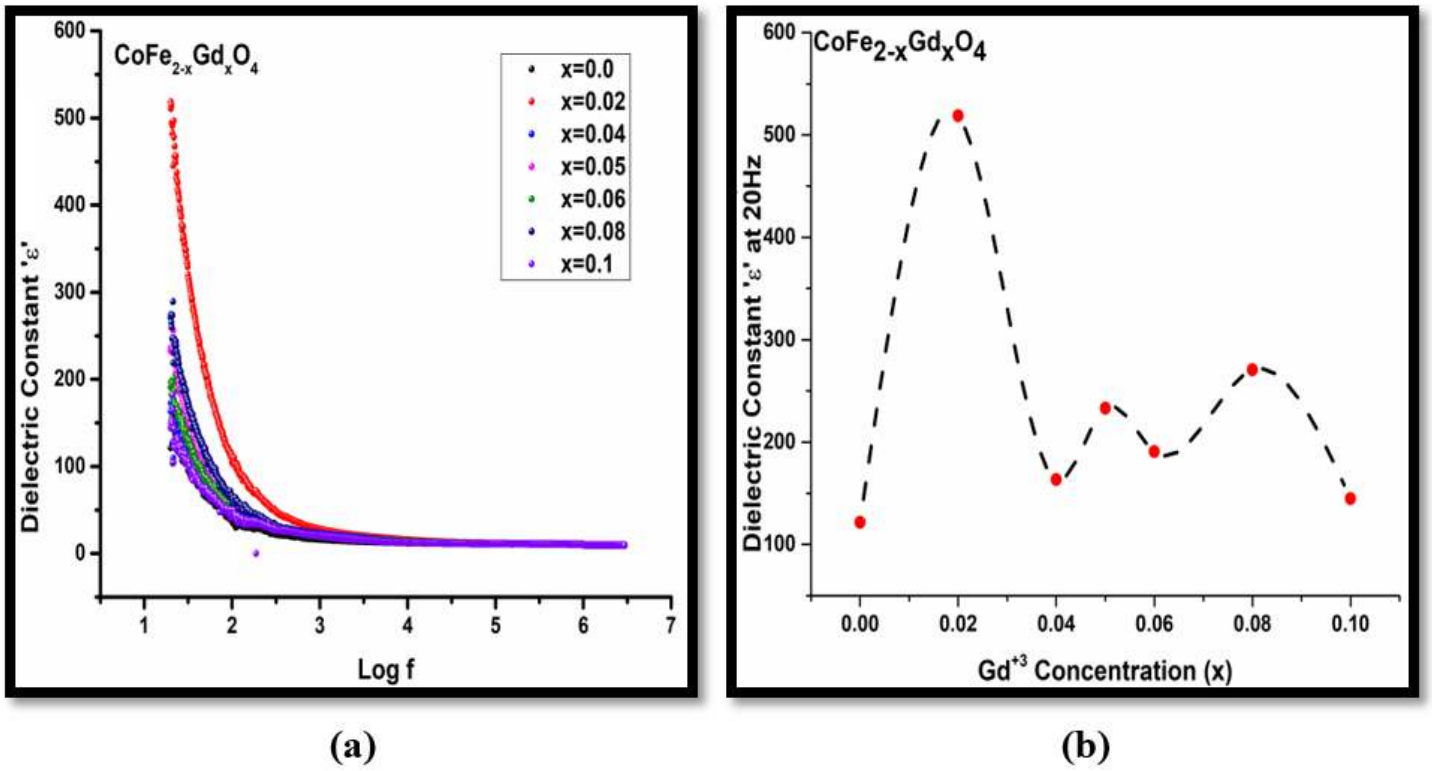

Figure 10

Variation of dielectric constant ‘ε’ (a) with frequency (b) at 20Hz

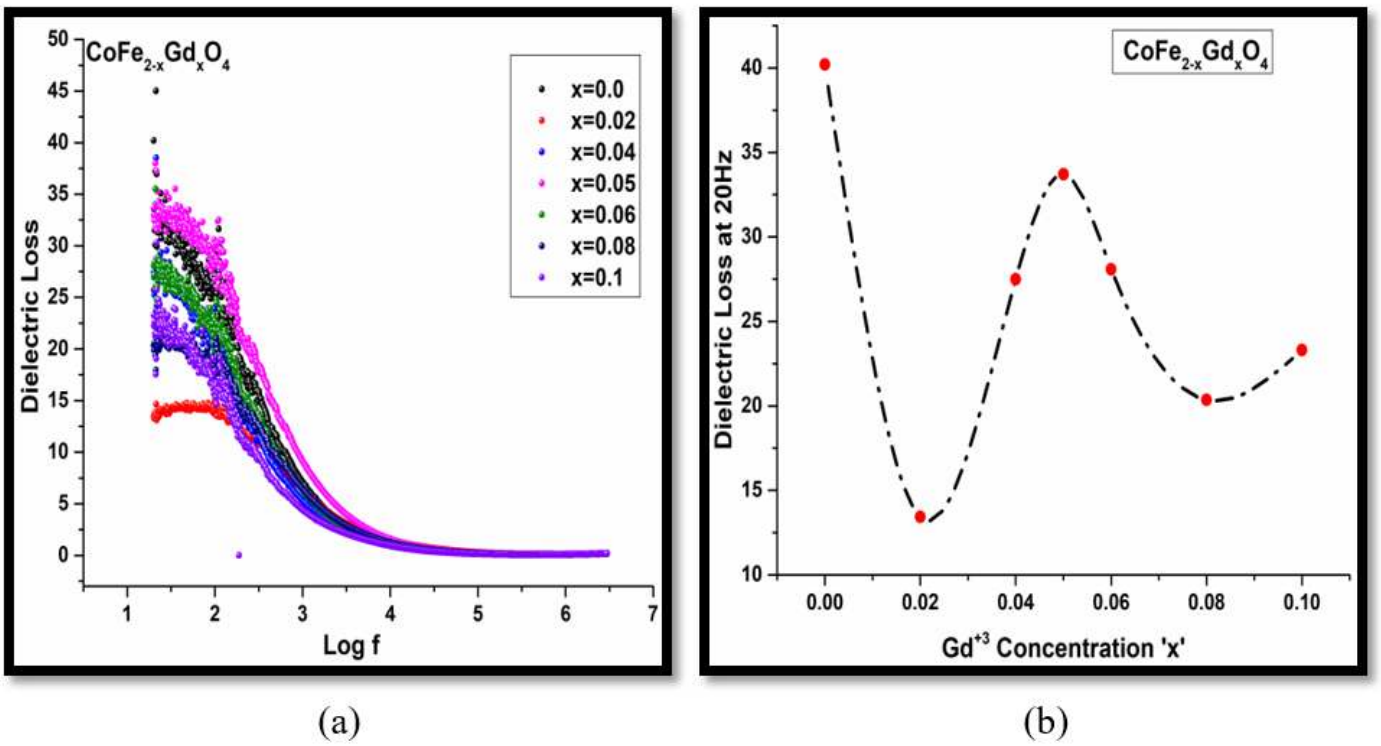

Figure 11

Variation of dielectric loss (a) with frequency (b) at 20Hz